Distinction between ice phases VII, VIII, and X

Graeme J. Ackland* and Andreas Hermann
Centre for Science at Extreme Conditions, School of Physics and Astronomy, University of Edinburgh, Edinburgh EH9 3FD, United Kingdom

Kazuki Komatsu
Geochemical Research Center, Graduate School of Science, The University of Tokyo, Japan

Keishiro Yamashita and J. S. Loveday
Centre for Science at Extreme Conditions, School of Physics and Astronomy, University of Edinburgh, Edinburgh EH9 3FD, United Kingdom

(Received 9 April 2025; accepted 29 August 2025; published 25 September 2025)

Ice phases VII, VIII, and X are all based on a body-centered cubic arrangement of molecules, the differences coming from how molecular orientation breaks the symmetry. It is debatable as to whether these should even be considered distinct phases given that the standard definition of a transition between distinct phases involves a discontinuity in any derivative of the free energy. This can be hard to prove experimentally, and most previous theoretical works have been based on models which either have continuously differentiable free energies or offer no straightforward way to determine the free energy. Here we build a free-energy model based on the common definitions of the phases: ordered ice-VIII, orientationally disordered ice VII, and centered-proton ice X. All transitions in this model might or might not be associated with a discontinuity in the specific heat, depending on parameterization. By comparing with data, we find that a VII-X transition line exists, but it ends in a critical point hidden within the stability field of phase VIII. If the model is correct, there is a discontinuity between VII and X, so they are separate phases. We propose that the hidden phase boundary might be demonstrated experimentally by compression of supercooled ice VII.

DOI: 10.1103/nmlm-rtxz

I. INTRODUCTION

There are currently at least twenty-two known crystalline phases of ice [1–3]. These phases are generally numbered with Roman numerals in the chronological order that they were discovered. The exception to this numbering system is ice I. The stable ambient pressure form is generally called ice I_h because it has a hexagonal structure. However, like the close-packed structures, a tetrahedral network like ice I has an alternative stacking which is cubic called ice I_c and a range of stacking fault disordered structures between the end members (ice I_{sd}) [4].

Other ice phases exist at high pressure. In the vast majority of these phases the water forms molecules in which an oxygen atom is strongly bound to two hydrogen atoms. With increasing pressure, a series of phases exists with increasing packing efficiency of the crystal structure. Typically, in a given pressure range, there is a high-temperature hydrogen-disordered phase and a low-temperature ordered phase with broken symmetry but similar topology. Very high pressure eventually breaks apart the strong molecular bonds [5].

A central concept for molecular ice structures is the Bernal-Fowler ice rules [6]:

(1) Each oxygen is covalently bonded to two hydrogen atoms with a bond angle around 105°.

(2) Each oxygen accepts precisely two hydrogen bonds from neighboring hydrogen atoms.

These two rules are insufficient to define the orientation of the water molecules for a given arrangement of the oxygen atoms uniquely. Therefore, ices tend to have a "Pauling entropy" associated with the number of possible arrangements, consistent with the ice rules [7]. The ice rules place long-range constraints on the number of arrangements depending on the crystal structure: a typical value of the Pauling entropy is around [7] 3.4 J mol^{-1} K^{-1}, but exact values are not known because the various arrangements have slightly different energies [8].

The phase diagram of water is shown in Fig. 1. In the region of the phase diagram below 100 GPa, ice VII occupies the largest portion [9]. At room temperature, ice VII forms at ≈2 GPa. Ice VII has a cubic structure in which oxygen atoms occupy cubic sites centered on the body (bcc) [10]. In the time- and space-averaged structure measured by diffraction, each oxygen atom is associated with four half-occupied hydrogen sites ≈1 Å away, arranged in a tetrahedron along four equivalent ⟨111⟩ directions. At least at low pressures (up to ≈15 GPa), where all evidence points to strongly bonded H_2O molecules, it is assumed ice VII obeys the ice rules. The average structure (shown in the inset of Fig. 2) with half-occupied

*http://www.ph.ed.ac.uk/~gja

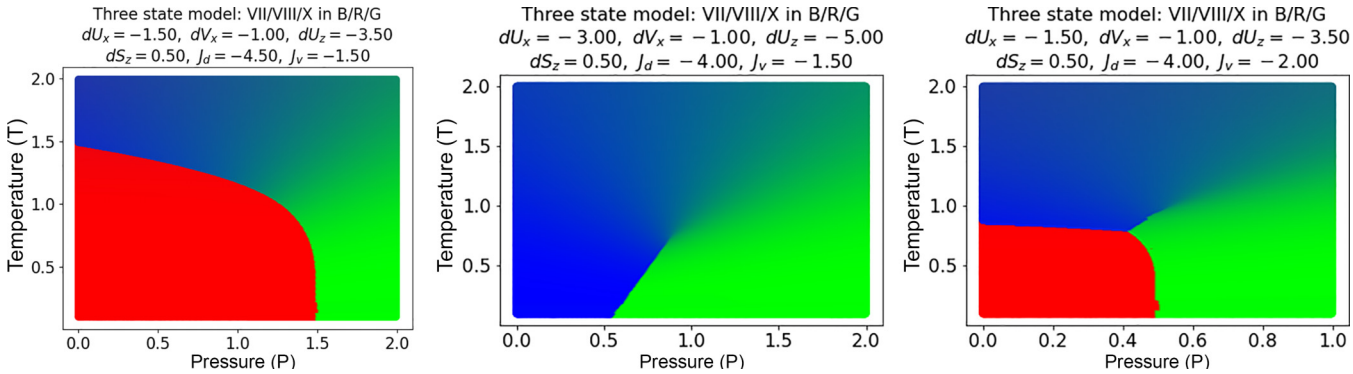

FIG. 1. Plot of relative amounts of VII (blue), VIII (red), X (green) with parameter sets chosen to illustrate three separate types of behavior allowed by the model. Solid lines show discontinuous changes associated with phase boundaries. (left) VII-X boundary and critical point hidden in phase VIII region. (center) Same model with phase VIII suppressed to reveal critical point. (right) VII-X boundary and critical point outside phase VIII region, and featuring VII-VIII-X triple point.

H sites is therefore the result of the molecules' orientations fluctuating. Ice VII is thus said to be "proton-disordered" which is written as half-atom "O–H/2 · · · H/2–O" configurations. The tetrahedral H-bond arrangement means that each oxygen is H-bonded to only four of its eight nearest neighbors. Hence ice VII has two interpenetrating and unconnected diamond-like networks of hydrogen-bonded water which give rise to a (111) Bragg peak in diffraction.[1] Ice VII has a configurational entropy significantly lower than implied by the ice rules (1.94 J mol^{-1} K^{-1} [16]).[2]

The search for nonmolecular phases beyond ice VII was a significant goal for high-pressure scientists [9,17–21]. Early reports [17,18] appear now to have detected other phenomena but there is now a consensus that spectroscopic studies [19,20] show the transition as starting at ≈60 GPa in H_2O and completing at ≈120 GPa. This consensus is supported by *ab initio* modeling [22–24]. The stability region of ice VII extends to the first nonmolecular phase, which was named ice X.

There is a consensus that ice X is a phase in which the hydrogen atoms cease to be covalently bonded to a single oxygen atom, instead being shared between two oxygens. Consequently, the molecular character of water is lost in ice X. But this proposed ice X has the same crystal symmetry as ice VII, so the structural marker of the transition from molecular to nonmolecular is difficult to define conceptually and even with access to neutron-diffraction data to measure experimentally [21]. As a result, a thermodynamics or crystallographic definition of the transition to ice X remains unclear.

In the pressure range 2–15 GPa (20 for D_2O) ice VII undergoes orientational ordering at ≈273 K to form ice VIII. In ice VIII the molecules in the two H-bonded networks order antiparallel to form a tetragonal antiferroelectric structure. Although ordering induces a small distortion of the ice VII structure, the principal features of the structures of ice VII and ice VIII is that they have the same basic oxygen arrangements and differ in that ice VIII has ordered H bonds (O–H· · · O) and ice VII disordered H bonds (O–/2 · · · H/2–O).

The ice VII/VIII boundary follows a near isotherm between 2 and ≈15 GPa. It then begins to fall with increasing pressure and then tends towards an isobar intersecting $T = 0$ at 60 (80 for D_2O) GPa [9]. The isotherm shows no significant isotope effect but, when the transition temperature begins to fall, there is an increasing isotope effect so that for a given ordering temperature D_2O orders at a higher pressure than does H_2O.

As has been stated, pressure has the eventual effect of breaking the covalent O–H bond, leading to the formation of nonmolecular ice X [19]. While there is a general consensus that this happens, there is no consensus as to where the transitions from the molecular forms (ices VII and VIII) to ice X are located. The merging of the two-site bonds (O–H/2 · · · H/2–O) of ice VII to the single -site bonds (O · · · H · · · O) of ice X is likely to be a continuous process and is very difficult to detect structurally. Similarly, there is a debate as to whether ordered ice VIII transforms directly to ice X at low temperatures or passes through a two-site ice VII state before reaching ice X as is seen in the analogous KH_2PO_4 system [25].

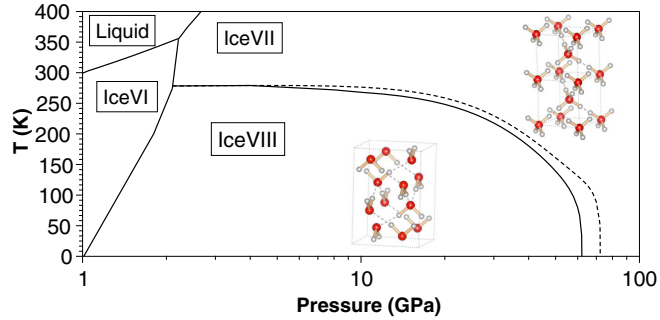

FIG. 2. Proposed phase diagram of water based on data taken from Ref. [9]. Solid (dashed) lines show phase-transition lines for H_2O (D_2O). Insets show antiferroelectric ice VIII and half-occupied sites in disordered ice VII.

[1]This also means the molecular positions are slightly displaced from bcc—(111) is forbidden in bcc. The basic structure of ice VII described here is further complicated by the existence of multisite disorder of both oxygen and hydrogen atoms [10–15]. These phenomena are noted for completeness and are not considered important to the thrust of this paper.

[2]There are arithmetic errors in the values given in Ref. [16]. This value has been calculated from the given Clapeyron slopes.

Ice X has been extensively modeled with density functional theory (DFT) [22,26–29]. If the protons are treated classically, the appearance of a single potential well does not occur until very high pressures, with the symmetric structure showing unstable phonons until well over 110 GPa [27,28]. At lower pressures two phonon instabilities occur. One is a flat band across the Brillouin zone (the local bond formation, equivalent to ice VII), and a second at the R point leading to the tetragonal $I4_1/amd$ structure of ice VIII [28]. This splitting has a signature in the infrared, which is dominated by anharmonic effects, which have been approximated by classical molecular dynamics plus Berry phase calculations [22], which are in qualitative agreement with experiment [19] except for a pressure offset around 30 GPa, which can be attributed to the symmetrizing effects of treating the protons quantum mechanically [23,29].

Despite the double-well potential persisting above 100 GPa, simulations using path integral MD, classical MD, and self-consistent phonons have revealed a centered probability distribution [29–32]. These simulations offer three distinct scenarios: at low pressure the proton is associated with one oxygen; in an intermediate regime, it has a double-peaked probability distribution and hops or resonates between the two; at higher pressure there is a single-peaked probability distribution, when the peak separation is less than the full width at half maximum (FWHM). All this means that the width of the distribution has a maximum in the intermediate regime.

A further transition to a distorted hcp structure (*Pbcm*) was proposed as ice XI in 1996 [33]. This was based on molecular dynamics started as bcc with only 16 molecules, which invariably forms a twinned structure due to stress generated on the Burgers path [34–36] and so can be interpreted as the fcc structure ice XVIII [37,38]. A superionic phase with the ice-VII like $Pn\bar{3}m$ symmetry was proposed [39], but was later renamed ice XX based on experimental optical conductivity measurements consistent with the calculation [40]. Very recently, a plastic-crystal form of ice VII near the melting point was reported [3,41], in which the reorientation time of the molecules approaches the libration period. Unlike the proposed phase XX, it appears the covalent H_2O molecules retain their integrity in the plastic crystal and that the time and space average structure maintains the $Pn\bar{3}m$ space group and the two H-bond networks of "normal" ice VII, as shown by the presence of the (111) reflection in neutron-diffraction data [3].

In addition to diffraction data which probe long-range order, spectroscopy is regarded as sufficient evidence for a phase transformation. While this is pragmatic, in a disordered system such as ice VII, the active modes are localized [42–44]. Ice VII may well contain molecules with a full shell of antiferromagnetic neighbors identical to ice-VIII—indeed this configuration is energetically and hence statistically favored and becomes increasingly more likely as the transition to phase VIII is approached.

The energetics of ice VII, VIII, X can therefore be attributed to two factors: the electrostatic arrangement favoring one orientation of the water dipole over another, and the energy required to break the covalent bond.

In thermodynamics, this leads to pressure-driven competition between the cost of covalent bonding and the density gain (VIII-X transition) and temperature-driven competition between the dipole energy loss and entropy gain (VIII-VII transition).

Here we build a minimal model which uses only these two contributions to define the three distinct phases.

II. BASIC IDEAS

In this paper we set out a thermodynamic framework in which to discuss the ice VII-VIII-X transitions. We work in dimensionless units: it is straightforward to rescale to fit the phase diagram and estimate parameters empirically later, but our aim is to describe *all possible* behaviors of the demolecularization transition.

We start by defining the three distinct phases from a theoretical point of view.

(1) The oxygen atoms in ice VII, VIII, and X form a network equivalent to the bcc lattice.

(2) The hydrogen-bonding network in ice VII, VIII, and X comprises two interpenetrating lattices.

(3) Ice VIII is a singly degenerate antiferroelectric ordered state consistent with the ice rules.

(4) Ice VII is a weighted average of states consistent with the ice rules.

(5) Ice X does not obey the ice rules. Each hydrogen atom is associated with two oxygens, but there is no asymmetry between the "covalent bond" and the "hydrogen bond."

The long-range ordering of the dipoles means that VIII has different crystal symmetry from VII and X. All phases have vibrational entropy, but ice VII also has finite configurational entropy: VIII and X are pure states with zero configurational entropy. Examples of these structures calculated by DFT in four-molecule cells have been used to analyze the transition mechanisms in the ice X region using graph theory [45].

At finite temperature, entropy will also mix the states, so our model considers the free energy of a system with a fraction x of ice X, y of ice VIII, and $z = (1 - x - y)$ of ice VII. We now consider phase transitions between the various phases. We use the standard Ehrenfest definition of a phase transition, whereby it corresponds to a discontinuous change in a derivative of the free energy, which implies a discontinuous change in x, y, z.

The equation of state is primarily determined by contributions which are essentially identical for all phases and not included here. So, to describe phase transitions, we must focus on *excess* free energy: Phase VIII is the easiest phase to calculate the free energy using DFT and quasiharmonic phonons, so we take G_{VIII} as our reference free energy, defining G_z and G_x as the excess free energies of phases VII and X relative to G_{VIII} (and similarly for other thermodynamic quantities).

The parameters in the model define contributions to the excess free energy. They are defined here as follows:

(1) zS_z is the excess entropy of phase VII, from permutations obeying the ice rules.

(2) zU_z is the excess energy of a typical phase VII microstate compared with phase VIII.

(3) $y^2 J_D$ is the antiferroelectric (dipole-dipole) energy of phase VIII; the y^2 term arises because it depends on the amount of y surrounding the site.

(4) $x(1-x)J_v$ is the enthalpy cost for mixing molecular and nonmolecular microstates.

(5) xU_x is the energy of ice X due to breaking the covalent bonds.

(6) xV_x is the reduced volume of phase X compared with VII and VIII.

For simplicity, the model makes some approximations which could be relaxed. All parameters are assumed independent of P and T, and the densities of phases VII and VIII are assumed equal.

Among these parameters, we can expect U_x to have a significant isotope effect, with a smaller value in hydrogen. This is because the higher zero-point energy makes the OH bond easier to break than the OD equivalent.

III. ICE VII-VIII TRANSITION

The transition from ice VII to VIII is first order and involves a change in symmetry. It is primarily driven by entropy. A statistical-mechanical treatment of this transition considering all the permutations of hydrogen bonding which obey the ice rules and building a partition function has been done [46]. Unfortunately, such a treatment cannot, even in principle, exhibit a phase transition because it only describes a single phase. It gives a crossover from ice VII-like to ice VIII-like behavior, with no discontinuities in the thermodynamic properties. There is no symmetry breaking because the partition function covers both phases and includes the antiferroelectric orientations of ice VIII along the crystalline axes. Even though there is no phase transformation, the approach allows a qualitative, and accurate, estimate of the phase boundary from the peak in specific heat.

To introduce a true phase transition, we make a mean-field free-energy model for VII-VIII by postulating that there is an antiferroelectric microstate with enthalpy H_{VIII} and other ice-rule-obeying microstates with excess energy U_z. We associate an excess entropy parameter S_z with ice VII.

We can then define the free-energy difference:

$$G_z = G_{\mathrm{VIII}} - G_{\mathrm{VII}} = J_D y^2 + zU_z - zTS_z. \tag{1}$$

J_D, U_z, and S_z parameters could be fitted to data or be calculated, the first two from DFT comparing many supercell configurations, and S_z using the Pauling entropy in ice VII or, equivalently, the latent heat. Implicit approximations here are that U_z and J_D are constants, meaning that all ice VII configurations have the same density and the electrostatic energy does not change with compression.

Dynamical considerations

We are primarily concerned with energetics rather than dynamics, so this section does not affect our other results. However, whether a "hidden" VII-X critical point in the ice-VIII stability region could be detected in practice depends on metastability and kinetics.

Transformations between different microstates of ice VII may happen by rotation of a single water molecule. This may involve generation and propagation of defects which break the ice rules [47]. However a much lower barrier is possible if the ice rules are not broken. The smallest such correlated rotation of molecules is around a ring (see Fig. 3) wherein all OH bonds point clockwise, and each rotates in a coordinated motion to point anticlockwise (or vice versa). In fully disordered ice VII, 1 in 32 six-membered rings are of this type.

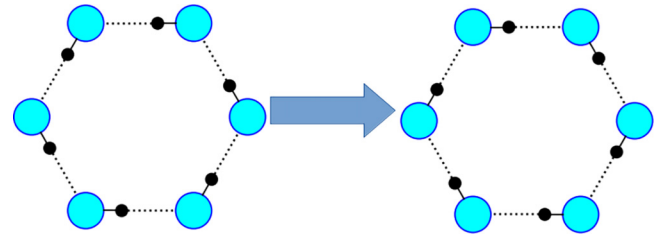

FIG. 3. Schematic mechanism transforming from one ice VII microstate to another using a ring where each water contributes one donor and one acceptor. Oxygens remain fixed, while hydrogen atoms move by rotation of the water molecules. If the dynamics proceeds by one rotation at a time, the first rotation creates a pair of ice-rule-breaking defects, subsequent rotations move the defects. If the rotation is simultaneous, no defect is created. Note that rings of this type do not exist in ice VIII. This figure serves a dual purpose: a single hydrogen in the left (right) figure can be taken to illustrate the basis functions Φ_L (Φ_R) for Eq. (2), with phase X a quantum superposition of the initial and final states.

By contrast, ice VIII has ferroelectric sublattices with no such directed loops, so it cannot be created from other ice VII configurations by such a correlated rotations. We postulate that the barrier between any ice VII microstate and ice VIII is higher than between ice VII microstates. Consequently, it is possible to define an ice VII partition function which excludes the ice VIII configuration. This implies that ice VII can be supercooled.

Ice VIII is antiferroelectric, which means that, on one sublattice, all molecules have their dipole moment oriented along the (001) axis. It may form domains or twins which we assume to be large enough that they do not contribute to the extensive free energy.

IV. ICE VIII-X TRANSITION

The ice VIII-X transition line goes vertically to the $T = 0$ axis, in accordance with the third law. The phase transformation is sometimes called a "quantum" phase transition and has a significant isotope effect.

We can define a single-site quantum system representing both phase VIII and phase X, using a superposition of two orthonormal basis states: the hydrogen covalently bonded to one or other oxygen (schematically shown in Fig. 3). We call these Φ_L and Φ_R (for left and right). These basis states represent two antiferroelectric domains of phase VIII, while phase X is a symmetric superposition $|c_L\Phi_L + c_R\Phi_R\rangle$ with c_L, c_R being the coefficients of the basis states. The mean hydrogen position in this mixed state is centered midway between the oxygens, although this position is not necessarily a maximum in the probability density: ice X may have either a one-peaked or two-peaked symmetric wave function

[27,29,30]. The two-peaked quantum probability distribution is sometimes misleadingly referred to with words implying time dependence such as "tunnelling" or "resonant."

To describe the *classical* disorder ice VII in this quantum model we would have to consider multiple sites, some of which have $c_L^2 = 1$ and others $c_R^2 = 1$. This adds additional complications which we will not pursue here.

We start by building the Hamiltonian for this system. We include (loss of) antiferroelectric energy at the self-consistent mean-field (SCF) level as in ice VII: U_z, and an exchange interaction enthalpy $-K_x$ describing bond breaking,[3] which increases as the overlap of the two states increases and also incorporates the increased density of ice X compared with VII and VIII:

$$\hat{H} = 2U_z\big(1 - |\phi_L\rangle c_L^2\langle\phi_L| - |\phi_R\rangle c_R^2\langle\phi_R|\big) - (|\phi_R\rangle c_R K_x c_L\langle\phi_L| + |\phi_L\rangle c_L K_x c_R\langle\phi_R|). \quad (2)$$

This gives zero for pure quantum states, then the first two terms represent the energy cost of breaking the ice rules, and second terms are the density gain from centering and the exchange interaction. Notice that this is a mean-field Hamiltonian which includes c_L and c_R from the interaction of the state with the local field. The excess enthalpy of a general state $(c_L|\Phi_L\rangle + c_R|\Phi_R\rangle)$ is then

$$H(c_L) = 2U_z\big(1 - c_L^4 - c_R^4\big) - 2K_x c_L^2 c_R^2 = 2c_L^2\big(1 - c_L^2\big)(2U_z - K_x), \quad (3)$$

where we have assumed that $c_L^2 + c_R^2 = 1$. Equation (3) gives excess enthalpy zero for ice VIII ($c_L = 1$ or 0) and $U_z - K_x/2$ for ice X ($c_L^2 = 1/2$). The expansion coefficients c_L and c_R are directly related to the phase fractions x, y, and z,

$$x = 2c_L c_R, \quad y + z = (c_L - c_R)^2. \quad (4)$$

The ambiguity in y and z is because ice VII and VIII are indistinguishable in this one-site model.

Converting quantum energy to excess thermodynamic enthalpy

To incorporate these ideas in a quantitative model, we first approximate the pressure dependence of K_x as linear: $K_x = K_0 + PV_x$: physically this means that the density difference between ice X and ice VIII is independent of pressure and volume. Finally, we combine the pressure independent terms to write $U_x = U_z - K_0/2$. This incorporates the idea that the VIII-X transition energy includes long-range antiferroelectric energy U_z and one-site bond-breaking energy K_0.

Since both phases are pure states, the phase line becomes vertical at $T = 0$, obeying the third law.

K_0 is the main source of isotopic effects. The OH bond has an associated vibrational frequency of more than 3300 cm^{-1} in H_2O, dropping to 2900 cm^{-1} in hydronium [48]. Deuterated water will be a factor of $\sqrt{2}$ lower, which implies a change in zero-point energy of around 0.025 eV, leading in turn to a significant isotope effect in the position of the phase line, as observed in the experiment. Detailed quasiharmonic calculation [46] also suggest that phonon effects give a 10% volume increase compared with the DFT enthalpy minimum, of which zero-point motion is the largest contribution.

As temperature increases, some of the disordered ice-VII states will be mixed into the ensemble. These will give rise to diffuse scattering and broadening of spectroscopic lines.

Even for simple choices of wave function and interaction, the self-consistent mean-field (SCF) term is extremely complicated and depends sensitively on the functional form chosen for the wave function. In principle, the SCF and basis functions can be back-derived, but we found the solutions are neither unique nor illuminating. Rather than guess some mathematical forms for the quantum wave functions and the SCF, then work from an ad hoc assumption to a precise but inaccurate energy, we choose to postulate the functional form of the excess enthalpy difference U_x.

V. ICE VII-X TRANSITION

We have developed well-defined thermodynamic models for the free-energy differences between VII-VIII and VIII-X. This allows us to finesse the microscopic definition of the VII-X transition. The free-energy difference between VII and X is simply $\Delta G_{\mathrm{VII-X}} = \Delta G_{\mathrm{VII-VIII}} - \Delta G_{\mathrm{VIII-X}}$.

VI. THERMODYNAMIC MODEL

We now put together all the concepts discussed above to build a unified thermodynamic model for the ice VII-VIII-X system. x, y, and z refer to the idealized phases VII, VIII, and X as described as above, but the actual system describes a linear combination of the three:

$$G(x, y, P, T) = G_{\mathrm{VIII}} + xG_x + zG_z + kT[x\ln x + y\ln y + z\ln z], \quad (5)$$

where the Roman-numeral-suffixed G_{VIII} denotes the full reference free energy, while G_x and G_z are the excess free energies above this.

A phase transition occurs when the fraction of a given component (x, y, z) changes discontinuously with T or P: this meets the standard Ehrenfest definition of a phase transition, a discontinuity in the first derivative of the free energy (entropy or volume).

In principle, each excess free energy includes energy, volume, and entropy terms, but following the discussion above we make some simplifying assumptions to reduce the parameter space.

(1) Phase VII has higher entropy, S_z being comprised of multiple microstates, phases VIII and X have the same entropy.

(2) Phase VIII is stabilized by the antiferroelectric dipole energy, provided by the mean field (fraction of phase VIII).

(3) Phase X has higher density, phases VII and VIII are similar.

(4) It is unfavorable to mix nonmolecular phase X with VII or VIII, since this causes long-range disruption to the ice rules.

[3]Notice that the physics here is similar to forming a chemical bond, except that here it is the proton rather than the electron shared between two atoms.

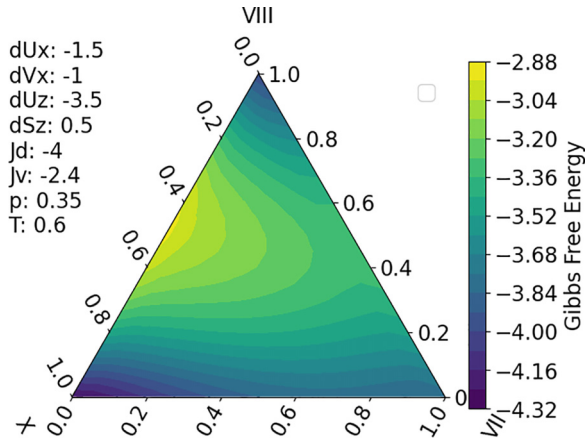

FIG. 4. $G(P, T, x, y)$ at selected P, T and model parameters illustrating the three local minima associated with phases VII, VIII, and X. The code to investigate different settings is available online [49].

Thus we can discover equilibrium phase boundaries as discontinuities in the parametrized free energy:

$$\begin{aligned} G(P,T,x,y) &= G_{\mathrm{VIII}} + y^2 J_D + x(1-x)J_V + (U_z - TS_z)(1-x-y) \\ &\quad + (U_x + PV_x)x + kT[x\ln x + y\ln y \\ &\quad + (1-x-y)\ln(1-x-y)], \end{aligned} \tag{6}$$

$$G(P,T) = \min_{x,y} G(P,T,x,y). \tag{7}$$

In practice, we do this numerically, by simply calculating $G(P, T, x, y)$ on a grid of x, y and picking the lowest value for P, T. These calculations are implemented in a PYTHON notebook available on request [49].

VII. RESULTS

A. Possible forms of the phase diagram

Our model allows us to calculate the thermodynamically possible behavior for the ice VII, VIII, X phase diagram. We consider only cases where the phase boundaries between VII and VIII, and between VIII and X, exist and meet, enclosing the ice VIII region at low T and P.

The boundary between VII and X also represents a first-order phase transition, which starts in the region where ice VIII is the stable phase and ends in a critical point. Depending on the parameters, this critical point may be hidden inside the ice VIII region, or there may be a triple point and a critical point, or the critical temperature may be so high that it lies beyond the scope of the model, in the melt or superionic. These situations are illustrated in Fig. 1.

B. Determining the phase boundaries

A first-order transition implies that there may be metastability of the various phases arising from local minima in the free-energy surface. In Fig. 4 we show a situation close to the triple point where there are three distinct free-energy minima close to the "ideal" phases VII, VIII, and X.

Three scenarios are shown in Fig. 1. The VII-VIII boundary is close to isothermal while the VIII-X is close to isobaric. In the left panel parameters are chosen so that there is no VII-X phase boundary, the right panel, with different parameters, shows the VII-X boundary extending from a triple point and ending in a critical point. The central panel uses the same parameters as the left, except phase VIII is suppressed by assigning it a high energy: this reveals the "hidden" VII-X phase line and associated critical point.

A thermodynamic phase transition implies discontinuous changes in the optimal values of (x, y, z) as a function of pressure and/or temperature. In Fig. 5 we show the values of these quantities along a subcritical isotherm for conditions corresponding to Fig. 1. Notice that (x, y, z) do not go rigorously to zero. The discontinuities and steady changes in the excess contribution to entropy and volume are also shown.

In high-pressure physics, the temperature and pressure are assumed to be the independent variables. Therefore the phase transitions are associated with discontinuous changes in the excess volume and entropy, given by

$$S = \frac{\partial}{\partial T_P} \min_{x,y} [G(P,T,x,y)], \quad V = \frac{\partial}{\partial P_T} \min_{x,y} [G(P,T,x,y)]. \tag{8}$$

These are calculated analytically and plotted in Fig. 6: the sharp transitions are evident. The second derivatives, related to excess heat capacity, thermal expansion, and compressibility, are plotted in Figs. 7 and 8. Recall that these are excess quantities relative to phase VIII. If such quantities were measured, the line for maximum dP/dS could be misinterpreted as a negative-slope "VII-X boundary," whereas the line of maximum dV/dP might be misinterpreted as a positive slope boundary.

Previous figures were in reduced units, so in Fig. 9 we show an *ab oculo* log-linear fit to the experimental phase diagram of dS/dP, the thermal expansion. The VII-VIII and VIII-X phase boundaries appear as bright yellow lines—in fact they are discontinuities, so the dashed appearance on the VII-VIII boundary arises from how close the grid point is to the singularity. Two different extremal (Widom) lines emanate from the turning point: these are associated with the supercritical VII-X transition. This illustrates that measurements of different quantities will give different "phase lines."

Raman spectroscopy is a convenient probe for this region of high-pressure ice. Our model does not allow us to calculate Raman frequencies, however, it is possible to make some estimates on the linewidths. Specifically, in a disordered solid, Raman modes become localized and each molecule is in a slightly different environment and therefore vibrates with a slightly different frequency [44,50–56]. Quite simply, these should be regarded as separate modes [57], but if they are too close to experimentally resolve, they appear as an additional broadening. There is an added complication that phase VII is itself disordered, which adds broadening α. Consequently, we can define an estimated linewidth from the relative amounts of the three phases:

$$\Delta\omega \sim \alpha z + xy + yz + xz. \tag{9}$$

Detailed calculation of linewidths is well beyond the scope of a thermodynamic model, but we observe that this increases

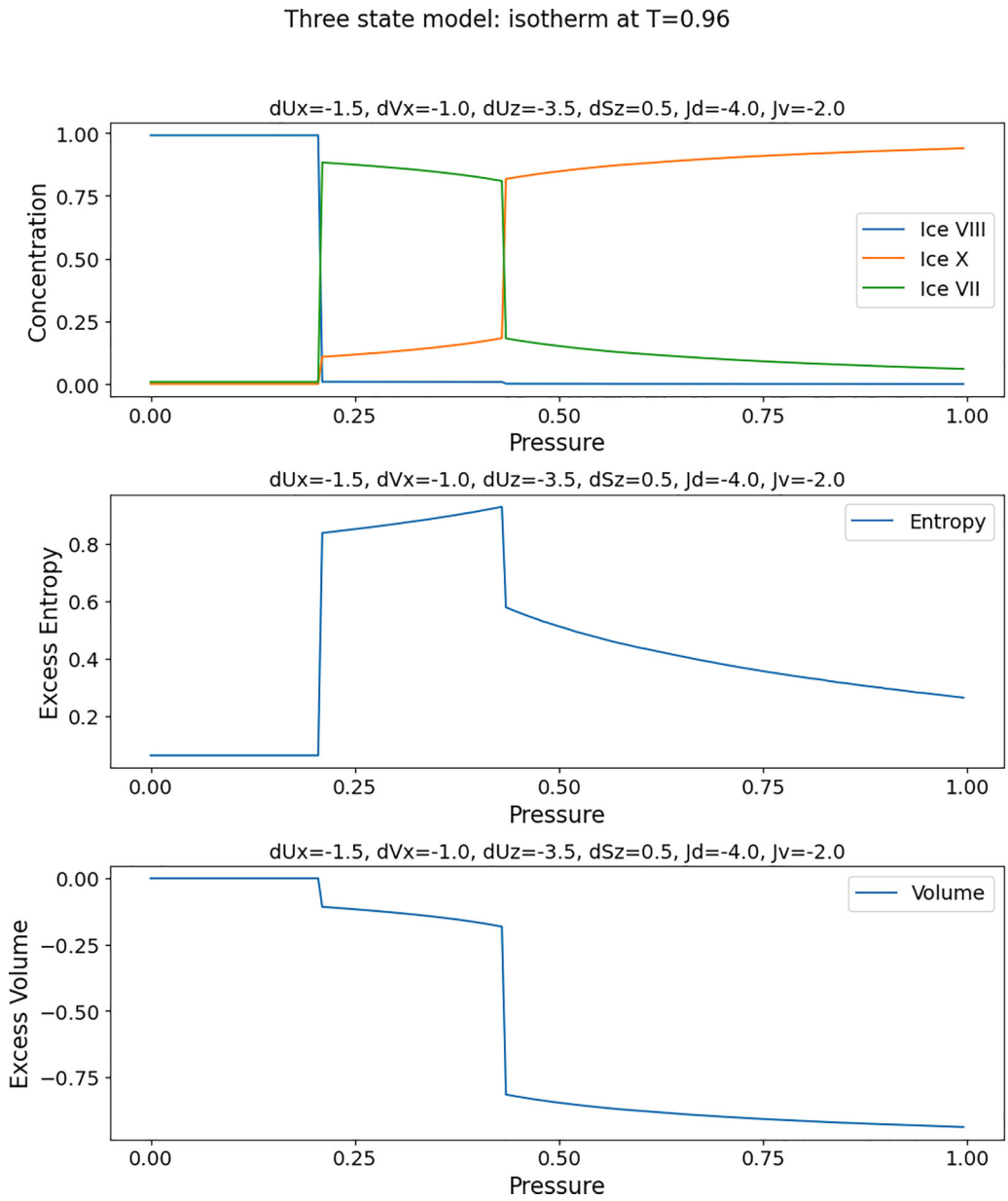

FIG. 5. Excess thermodynamic properties along an isotherm at $T = 0.85$. Fractions of ice VIII, VII, and X, excess entropy, excess volume.

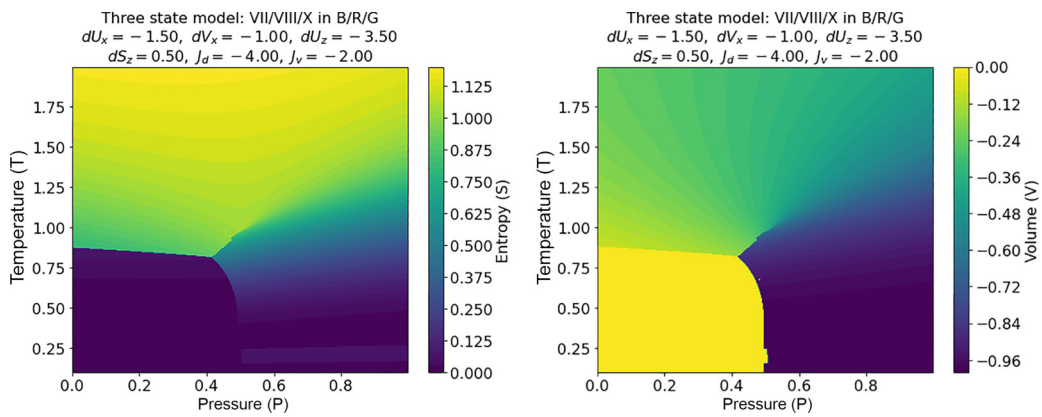

FIG. 6. (left) 2D plot of excess V vs T, P. (right) 2D plot of excess S vs T, P. The parameters here correspond to those in Fig. 1(b).

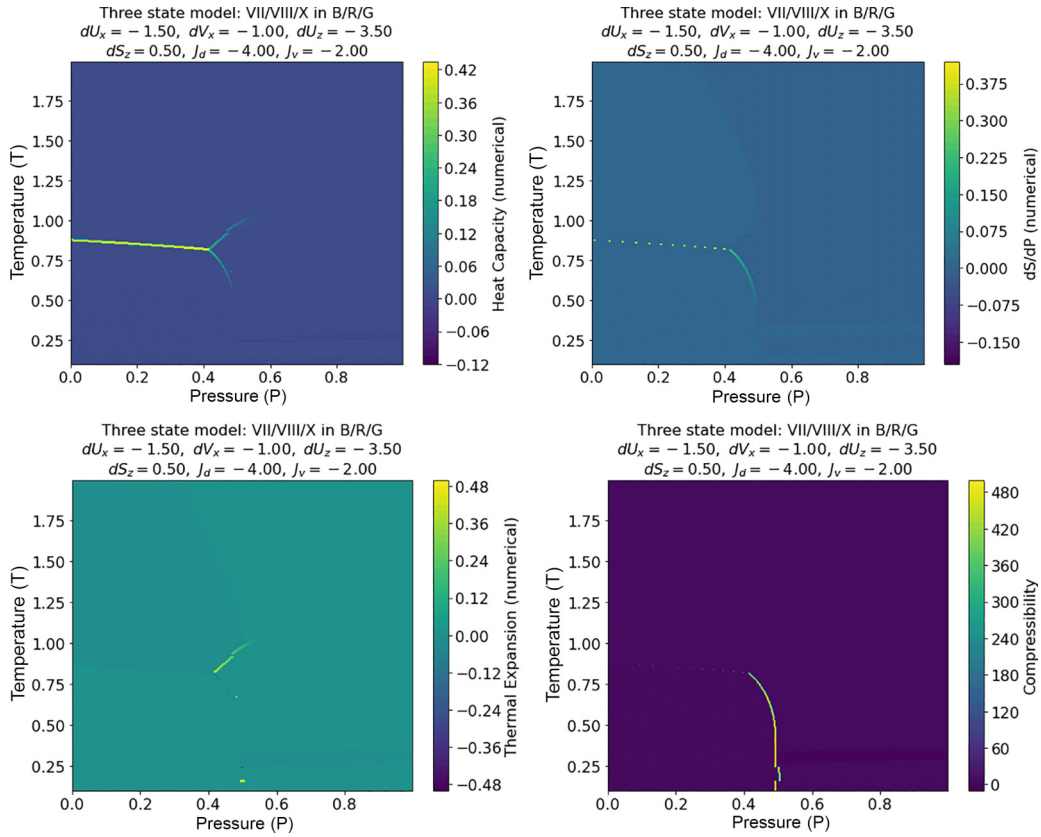

FIG. 7. Excess contribution to second derivatives of the Gibbs free energy, equivalent to the heat capacity, thermal expansion, and compressibility on a grid of P, T values. On a linear scale, the phase boundaries are clearly defined: they are in theory divergent but merely large when evaluated numerically.

with temperature, and as the phase boundary is approached (Fig. 10).

We can estimate the behavior of the O–H stretch, which defines the transformation to phase X. This should be related to the depth of the potential well: a double-well for phase VII and a single well for phase X. Precisely at the transition for such a model, the force constant goes to zero as does the frequency in the harmonic approximation: within our model, the frequency depends on the enthalpy difference between phase X and VII, which shows a minimum at the transition. In reality there is some anharmonic contribution and the system has a range of ice-X- and ice-VII-like environments, so it is

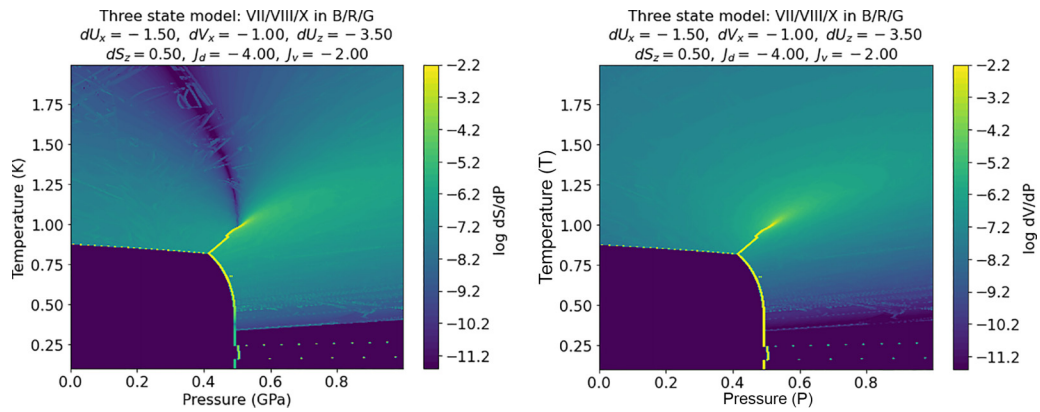

FIG. 8. Second derivatives of the Gibbs free energy, equivalent to thermal expansion and compressibility with absolute values shown on a log scale. Extrema in these quantities, which can be seen extending beyond the critical point, represent Widom lines. The dark blue line in the thermal expansion related dS/dP comes from the change from positive to negative thermal expansion. Note that the Maxwell relation $d^2G/dPdT = \partial S/\partial P_T = \partial V/\partial T_P$ means there are only three inequivalent second derivatives. The scale is truncated so that all very low values appear as solid dark blue at low temperature. The zero thermal expansion line is coincident with $x = z$ which we interpret as the minimum value for the Raman frequency.

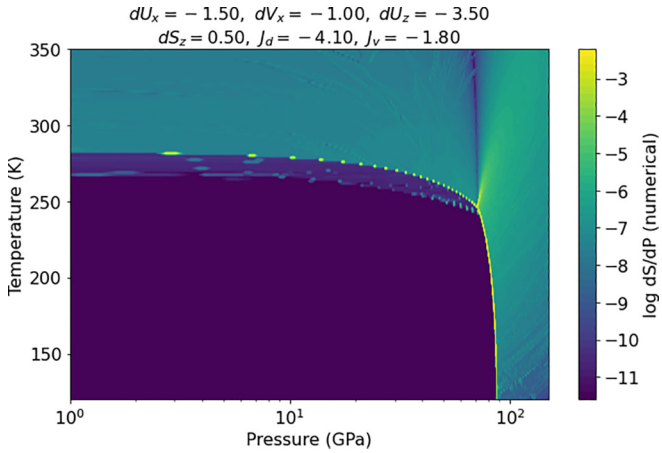

FIG. 9. Example of parametrization similar to experiment. The first-order boundary between phases VII and X ends at a critical point hidden in the ice VIII phase. The plotted quantity is a surrogate for possible measurements. The first-order VIII-VII and VIII-X boundaries are clear, the dotted appearance being an artifact arising from how close to the boundary the P, T grid points fall. The key observation is that measurement of the VII-X "boundary" may detect the yellow line or the blue line, depending on what experimental signal is used to "detct" the boundary. The are extrema in the thermodynamic quantity: neither is a discontinuity, but either could easily be interpreted as **the** phase boundary.

impossible to make a more qualitative prediction. However, we can note that the softening of the phonon occurs in both subcritical and supercritical regions, so it should not be used to determine whether there is a discontinuous thermodynamic transition.

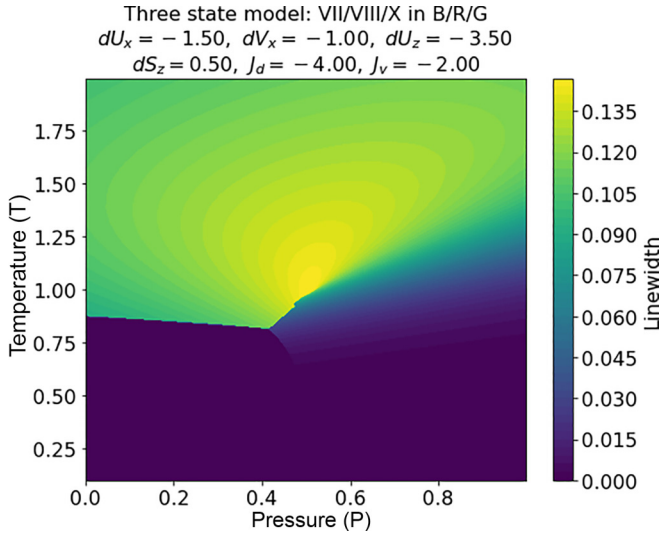

FIG. 10. Plot of the function $\alpha y + xy + xz + yz$ with $\alpha = 0.25$, which is related to the estimated Raman linewidth. The important feature of this is the increased linewidth in the supercritical region. If this is interpreted as the ice VII-X transition, then the line is close to an isobar, in contrast with the thermodynamic boundary and the Widom lines which have a modest, positive Clapeyron slope.

VIII. DISCUSSION

A. When is a phase boundary not a phase boundary?

One cannot measure an infinite quantity in an experiment, so in practice, phase lines are determined from maxima or rapid changes in some measurable quantity.

Widom lines are maxima in thermodynamic quantities such as specific heat, thermal expansivity, compressibility and they extend beyond the VII-X critical point. They should not be interpreted as the phase boundary, either theoretically (because they are not discontinuities) or experimentally (because different measurable quantities have different Widom lines). Figure 7 maps the various Widom lines that extend from the critical-point phase VII/X. Notice that these lines exist even if the critical point itself lies in the stability field of phase VIII. A best fit of the model to the experimental data, Fig. 9 suggests that the critical point is indeed hidden.

B. Raman modes

One of the main probes for the putative VII-X transition is Raman spectroscopy. Our thermodynamic model cannot calculate Raman frequencies, but we can make a qualitative model based on the relative amounts of ice VII and X. We propose that the minimum frequency of the O–H stretch will occur when $x = z$ (at $x + z \approx 1$). In our model, this is essentially coincident with the line of zero thermal expansion and close to an isobar.

C. Isotope effects

Isotopic effects are incorporated in the model via the parameter U_z. The effect of increasing U_z (deuteration) is to destabilize phase X, and move its phase boundaries to higher pressures in H_2O than in D_2O. This gives a strong isotope effect in the VIII-X boundary and a weak effect at the VII-VIII boundary.

For some choice of parameters, it is possible to "hide" the VII-X critical point in the phase VIII stability region for D_2O but not for H_2O. However, this requires fine tuning of the model and probably does not correspond to real ices.

D. Implications for interpreting experiments on the ice VII-X transition

In the supercritical VII-X region, it is likely that experimental probes will detect extrema in measured quantities which could be used to draw a line. However, the position of such a line is not unique: it depends on the experimental method being used. Most obviously from a thermodynamic viewpoint are the Widom lines seen from changes in compressibility (density), specific heat (entropy), and thermal expansion.

Other experimental probes, such as spectroscopic measures are even more indirect. There will be sharp changes at the phase boundary below the critical point, but even in the supercritical region there will be rapid changes in frequency with increased pressure from ice VII-like to ice-X-like regions. With a finite set of pressure points, a line may be drawn between the most different spectra. However, above the critical point this will not correspond to a phase transition and will

not be colocated with lines drawn based on other experimental data. Changes in linewidths are also expected, but again do not signify a phase boundary.

The zero of thermal expansion corresponds to the condition $x = z$ in the supercritical region (equal amounts of ice VII and X). It is not a Widom line, and does not resemble an extrapolation of the VII-X boundary. However, it does emanate from the critical point, even when the critical point is hidden. We propose that it corresponds to the minimum in the O–H stretch frequency, and explains the near-vertical phase boundary reported from that feature in Raman spectroscopy. Like the near isobaric VIII-X boundary, this is associated with the ease of breaking the O–H bonds, and will therefore have a significant isotope effect (U_x).

Consequently, the model shows that the position and shape of VII-X boundary depend on the probe used. It is possible to define a thermodynamic boundary based on the extrapolations from the hidden critical point: such a line has a modest Clapeyron slope from a balance between the higher entropy of phase VII and the higher density of phase X. By contrast, a more local probe such as spectroscopy is insensitive to the configurational entropy, and will suggest a more vertical phase boundary.

E. Realistic parameters

The experimental situation appears to be closest to the "hidden critical point," with no thermodynamic discontinuity to uniquely define the phase boundary. In the absence of convincing crystallographic evidence, claims for the transition are based on spectroscopy, which the model shows will give a near-vertical "crossover" boundary, in sharp contrast with the thermodynamics boundary.

F. Detectability of the hidden VII-X phase line

Below 10 GPa the VII-VIII transition kinetics are sluggish [58], perhaps because cooperative ring-reorientations (Fig. 3) do not provide a transformation path to these states. Changing the hydrogen-bonding arrangement of ice VII cannot be attained by single molecule rotations, without breaking the ice rules. A cooperative reorientation around a six-membered ring is required (Fig. 3). However, even this mechanism cannot reach the ice VIII arrangement. Such supercooled ice VII could be pressurized across the metastable phase boundary into ice X. However, the ice-X-like centering of the hydrogens eliminates the ice rules. Therefore, our model implies that, if metastable ice VII is compressed across the hidden phase boundary into ice X, the metastable ice X will rapidly transform to ice VIII.

IX. CONCLUSIONS

This paper set out to determine whether "phase X" should be regarded as a phase distinct from ice VII. We made a model with precise definitions of these two phases (and ice VIII) based on theoretical models. Within the model, ice VII and ice X are distinct thermodynamic phases separated by a phase boundary ending in a critical point. Comparison with experimental results suggests a parametrization for which the critical point lies in the region of phase VIII, and by implication the reported measurements lie in the supercritical region (Fig. 9). In this case, there is no discontinuity in density, and quantities such as Widom lines, frequency maxima, or abrupt linewidth changes will occur along different lines in P, T space. Hence different experimental probes may report systematically different transition or crossover "lines."

Historically, theoretical predictions have not been deemed sufficient to allocate a roman numeral to an ice phase. Whether the existing observations of ice VII or X in the supercritical region constitute observations of two distinct phases is essentially a matter of definition.

ACKNOWLEDGMENTS

This work was supported by the Engineering and Physical Sciences Research Council under Grants No. EP/Y020987/1 and No. EP/X035891/1, by the ERC Hecate Grant and by JSPS KAKENHI (Grant No. 21K18154).

DATA AVAILABILITY

The data that support the findings of this article are openly available [59].

[1] K. Komatsu, S. Machida, F. Noritake, T. Hattori, A. Sano-Furukawa, R. Yamane, K. Yamashita, and H. Kagi, Ice I_c without stacking disorder by evacuating hydrogen from hydrogen hydrate, Nat. Commun. **11**, 464 (2020).

[2] C. G. Salzmann, J. S. Loveday, A. Rosu-Finsen, and C. L. Bull, Structure and nature of ice XIX, Nat. Commun. **12**, 3162 (2021).

[3] M. Rescigno, A. Toffano, U. Ranieri, L. Andriambariarijaona, R. Gaal, S. Klotz, M. M. Koza, J. Ollivier, F. Martelli, J. Russo, F. Sciortino, J. Teixeira, and L. E. Bove, Observation of plastic ice VII by quasi-elastic neutron scattering, Nature (London) **640**, 662 (2025).

[4] T. L. Malkin, B. J. Murray, A. V. Brukhno, J. Anwar, and C. G. Salzmann, Structure of ice crystallized from supercooled water, Proc. Natl. Acad. Sci. USA **109**, 1041 (2012).

[5] W. B. Holzapfel, On the symmetry of the hydrogen bonds in ice VII, J. Chem. Phys. **56**, 712 (1972).

[6] J. D. Bernal and R. H. Fowler, A theory of water and ionic solution, with particular reference to hydrogen and hydroxyl ions, J. Chem. Phys. **1**, 515 (1933).

[7] L. Pauling, The structure and entropy of ice and of other crystals with some randomness of atomic arrangement, J. Am. Chem. Soc. **57**, 2680 (1935).

[8] C. P. Herrero and R. Ramírez, Configurational entropy of hydrogen-disordered ice polymorphs, J. Chem. Phys. **140**, 234502 (2014).

[9] P. Pruzan, J. C. Chervin, E. Wolanin, B. Canny, M. Gauthier, and M. Hanfland, Phase diagram of ice in the VII-VIII-X domain. Vibrational and structural data for strongly compressed ice VIII, J. Raman Spectrosc. **34**, 591 (2003).

[10] W. F. Kuhs, J. L. Finney, C. Vettier, and D. V. Bliss, Structure and hydrogen ordering in ices VI, VII, and VIII by neutron powder diffraction, J. Chem. Phys. **81**, 3612 (1984).
[11] J. D. Jorgensen and T. G. Worlton, Disordered structure of D2O ice VII from *in situ* neutron powder diffraction, J. Chem. Phys. **83**, 329 (1985).
[12] R. Nelmes, J. Loveday, W. Marshall, G. Hamel, and J. Besson, Multisite disordered structure of ice VII to 20 GPa, Phys. Rev. Lett. **81**, 2719 (1998).
[13] K. Yamashita, K. Komatsu, S. Klotz, O. Fabelo, M. T. Fernández-Díaz, J. Abe, S. Machida, T. Hattori, T. Irifune, T. Shinmei, K. Sugiyama, T. Kawamata, and H. Kagi, Atomic distribution and local structure in ice VII from *in situ* neutron diffraction, Proc. Natl. Acad. Sci. USA **119**, e2208717119 (2022).
[14] S. J. Singer, J.-L. Kuo, T. K. Hirsch, C. Knight, L. Ojamäe, and M. L. Klein, Hydrogen-bond topology and the ice VII/VIII and ice Ih/XI proton-ordering phase transitions, Phys. Rev. Lett. **94**, 135701 (2005).
[15] Z. Futera and N. J. English, Pressure dependence of structural properties of ice VII: An *ab initio* molecular-dynamics study, J. Chem. Phys. **148**, 204505 (2018).
[16] G. P. Johari, A. Lavergne, and E. Whalley, Dielectric properties of ice VII and VIII and the phase boundary between ice VI and VII, J. Chem. Phys. **61**, 4292 (1974).
[17] K. R. Hirsch and W. B. Holzapfel, Symmetric hydrogen bonds in ice X, Phys. Lett. A **101**, 142 (1984).
[18] A. Polian and M. Grimsditch, New high-pressure phase of H_2O ice X, Phys. Rev. Lett. **52**, 1312 (1984).
[19] A. F. Goncharov, V. V. Struzhkin, M. S. Somayazulu, R. J. Hemley, and H. K. Mao, Compression of ice to 210 gigapascals: Infrared evidence for a symmetric hydrogen-bonded phase, Science **273**, 218 (1996).
[20] A. F. Goncharov, V. V. Struzhkin, H.-K. Mao, and R. J. Hemley, Raman spectroscopy of dense H_2O and the transition to symmetric hydrogen bonds, Phys. Rev. Lett. **83**, 1998 (1999).
[21] K. Komatsu, T. Hattori, S. Klotz, S. Machida, K. Yamashita, H. Ito, H. Kobayashi, T. Irifune, T. Shinmei, A. Sano-Furukawa, and H. Kagi, Hydrogen bond symmetrisation in D_2O ice observed by neutron diffraction, Nat. Commun. **15**, 5100 (2024).
[22] M. Bernasconi, P. L. Silvestrelli, and M. Parrinello, *Ab initio* infrared absorption study of the hydrogen-bond symmetrization in ice, Phys. Rev. Lett. **81**, 1235 (1998).
[23] Y. Bronstein, P. Depondt, F. Finocchi, and A. M. Saitta, Quantum-driven phase transition in ice described via an efficient Langevin approach, Phys. Rev. B **89**, 214101 (2014).
[24] J. A. Hernandez and R. Caracas, Proton dynamics and the phase diagram of dense water ice, J. Chem. Phys. **148**, 214501 (2018).
[25] R. J. Nelmes, M. I. Mcmahon, R. O. Piltz, and N. G. Wright, High-pressure neutron-diffraction studies of KH_2PO_4-type phase-transitions as T_c tends to 0 K, Ferroelectrics **124**, 355 (1991).
[26] M. Benoit, D. Marx, and M. Parrinello, The role of quantum effects and ionic defects in high-density ice, Solid State Ionics **125**, 23 (1999).
[27] M. Benoit, A. H. Romero, and D. Marx, Reassigning hydrogen-bond centering in dense ice, Phys. Rev. Lett. **89**, 145501 (2002).
[28] M. Marqués, G. J. Ackland, and J. S. Loveday, Nature and stability of ice X, High Pressure Res. **29**, 208 (2009).
[29] M. Benoit, D. Marx, and M. Parrinello, Tunnelling and zero-point motion in high-pressure ice, Nature (London) **392**, 258 (1998).
[30] D. Kang, J. Dai, H. Sun, Y. Hou, and J. Yuan, Quantum simulation of thermally-driven phase transition and oxygen *k*-edge x-ray absorption of high-pressure ice, Sci. Rep. **3**, 3272 (2013).
[31] M. Cherubini, L. Monacelli, B. Yang, R. Car, M. Casula, and F. Mauri, Quantum effects in H-bond symmetrization and in thermodynamic properties of high pressure ice, Phys. Rev. B **110**, 014112 (2024).
[32] J. Tsuchiya, M. Shiga, S. Tsuneyuki, and E. C. Thompson, Nuclear quantum effect on the elasticity of ice VII under pressure: A path-integral molecular dynamics study, Phys. Rev. Res. **6**, 023302 (2024).
[33] M. Benoit, M. Bernasconi, P. Focher, and M. Parrinello, New high-pressure phase of ice, Phys. Rev. Lett. **76**, 2934 (1996).
[34] U. Pinsook and G. J. Ackland, Simulation of martensitic microstructural evolution in zirconium, Phys. Rev. B **58**, 11252 (1998).
[35] U. Pinsook and G. J. Ackland, Atomistic simulation of shear in a martensitic twinned microstructure, Phys. Rev. B **62**, 5427 (2000).
[36] U. Pinsook and G. J. Ackland, Calculation of anomalous phonons and the hcp-bcc phase transition in zirconium, Phys. Rev. B **59**, 13642 (1999).
[37] G. Weck, J.-A. Queyroux, S. Ninet, F. Datchi, M. Mezouar, and P. Loubeyre, Evidence and stability field of fcc superionic water ice using static compression, Phys. Rev. Lett. **128**, 165701 (2022).
[38] M. Millot, F. Coppari, J. R. Rygg, A. Correa Barrios, S. Hamel, D. C. Swift, and J. H. Eggert, Nanosecond x-ray diffraction of shock-compressed superionic water ice, Nature (London) **569**, 251 (2019).
[39] C. Cavazzoni, G. Chiarotti, S. Scandolo, E. Tosatti, M. Bernasconi, and M. Parrinello, Superionic and metallic states of water and ammonia at giant planet conditions, Science **283**, 44 (1999).
[40] V. B. Prakapenka, N. Holtgrewe, S. S. Lobanov, and A. F. Goncharov, Structure and properties of two superionic ice phases, Nat. Phys. **17**, 1233 (2021).
[41] A. Toffano, J. Russo, M. Rescigno, U. Ranieri, L. E. Bove, and F. Martelli, Temperature-and pressure-dependence of the hydrogen bond network in plastic ice VII, J. Chem. Phys. **157**, 094502 (2022).
[42] B. Minceva-Sukarova, W. F. Sherman, and G. R. Wilkinson, The Raman spectra of ice (Ih, II, III, V, VI and IX) as functions of pressure and temperature, J. Phys. C: Solid State Phys. **17**, 5833 (1984).
[43] P. Pruzan, J. Chervin, and M. Gauthier, Raman spectroscopy investigation of ice and deuterated ice VII to 40 GPa. Disorder in ice VII, Europhys. Lett. **13**, 81 (1990).
[44] M. Frost, A. Hermann, S. H. Glenzer, and G. J. Ackland, Isotopic Raman broadening due to Anderson localization of harmonic phonons in partially deuterated ice VII and VIII, Phys. Rev. Res. **5**, 043166 (2023).
[45] L. Li, P. Gao, W. Zhang, G. Liu, J. Lv, and Y. Wang, Phase transitions of ice VIII-VII-X: A potential energy landscape perspective, Phys. Rev. Res. **6**, 043085 (2024).
[46] K. Umemoto, R. M. Wentzcovitch, S. De Gironcoli, and S. Baroni, Order–disorder phase boundary between ice VII and

VIII obtained by first principles, Chem. Phys. Lett. **499**, 236 (2010).
[47] N. Bjerrum, Structure and properties of ice, Science **115**, 385 (1952).
[48] M. Falk and P. A. Giguère, Infrared spectrum of the H_3O^+ ion in aqueous solutions, Can. J. Chem. **35**, 1195 (1957).
[49] See Supplemental Material at http://link.aps.org/supplemental/10.1103/nmlm-rtxz for additional figures similar to Figs. 1, 4–10 using different parameterizations can be generated and explored using the code [59]. The rendering of Eqs. (1)–(9) in code is also available there.
[50] P. I. C. Cooke, I. B. Magdău, M. Pena-Alvarez, V. Afonina, P. Dalladay-Simpson, X.-D. Liu, R. T. Howie, E. Gregoryanz, and G. J. Ackland, Raman signal from a hindered hydrogen rotor, Phys. Rev. B **102**, 064102 (2020).
[51] P. I. Cooke, I. B. Magdău, and G. J. Ackland, Calculating the Raman signal beyond perturbation theory for a diatomic molecular crystal, Comput. Mater. Sci. **210**, 111400 (2022).
[52] S. B. Ramsey, M. Pena-Alvarez, and G. J. Ackland, Localization effects on the vibron shifts in helium-hydrogen mixtures, Phys. Rev. B **101**, 214306 (2020).
[53] I. B. Magdău and G. J. Ackland, Identification of high-pressure phases III and IV in hydrogen: Simulating Raman spectra using molecular dynamics, Phys. Rev. B **87**, 174110 (2013).
[54] M. Peña-Alvarez, V. Afonina, P. Dalladay-Simpson, X.-D. Liu, R. T. Howie, P. I. Cooke, I. B. Magdau, G. J. Ackland, and E. Gregoryanz, Quantitative rotational to librational transition in dense H2 and D2, J. Phys. Chem. Lett. **11**, 6626 (2020).
[55] R. T. Howie, I. B. Magdău, A. F. Goncharov, G. J. Ackland, and E. Gregoryanz, Phonon localization by mass disorder in dense hydrogen-deuterium binary alloy, Phys. Rev. Lett. **113**, 175501 (2014).
[56] G. J. Ackland and J. S. Loveday, Structures of solid hydrogen at 300 K, Phys. Rev. B **101**, 094104 (2020).
[57] I. B. Magdău and G. J. Ackland, Infrared peak splitting from phonon localization in solid hydrogen, Phys. Rev. Lett. **118**, 145701 (2017).
[58] K. Komatsu, S. Klotz, S. Machida, A. Sano-Furukawa, T. Hattori, and H. Kagi, Anomalous hydrogen dynamics of the ice VII–VIII transition revealed by high-pressure neutron diffraction, Proc. Natl. Acad. Sci. USA **117**, 6356 (2020).
[59] https://git.ecdf.ed.ac.uk/aherman2/three-ices-model.